

Multi-Skyrmions on $AdS_2 \times S_2$, Rational maps and Popcorn transitions

Fabrizio Canfora¹, Gianni Tallarita²

¹*Centro de Estudios Científicos (CECS), Casilla 1469, Valdivia, Chile.*

²*Departamento de Ciencias, Facultad de Artes Liberales, Universidad Adolfo Ibáñez, Santiago 7941169, Chile*

canfora@cecs.cl, gianni.tallarita@uai.cl

November 22, 2021

Abstract

By combining two different techniques to construct multi-soliton solutions of the (3+1)-dimensional Skyrme model, the generalized hedgehog and the rational map ansatz, we find multi-Skyrmion configurations in $AdS_2 \times S_2$. We construct Skyrmonic multi-layered configurations such that the total Baryon charge is the product of the number of kinks along the radial AdS_2 direction and the degree of the rational map. We show that, for fixed total Baryon charge, as one increases the charge density on $\partial(AdS_2 \times S_2)$, it becomes increasingly convenient energetically to have configurations with more peaks in the radial AdS_2 direction but a lower degree of the rational map. This has a direct relation with the so-called holographic popcorn transitions in which, when the charge density is high, multi-layered configurations with low charge on each layer are favored over configurations with few layers but with higher charge on each layer. The case in which the geometry is $M_2 \times S_2$ can also be analyzed.

1 Introduction

One of the most intriguing theoretical results in Quantum Field Theory (QFT henceforth) has been the realization that fermions can emerge out of a purely Bosonic Lagrangian as solitonic excitations (for a detailed review see [1]). The clearest demonstration of the importance of this result, which goes far beyond theoretical physics, is given by Skyrme's theory [2] which is one of the most important models of nuclear and particles physics. The inclusion of the famous Skyrme term [2] allows the existence of static soliton solutions of the pion non-linear sigma model with finite energy, called *Skyrmions* (see [3] [4] [5] [6]) describing Fermionic degrees of freedom (see [7] [8] [9] [10] [11] [12] [13] [14] [15] and references therein). Furthermore, the wide range of applications of this theory in other areas (such as astrophysics, Bose-Einstein condensates, nematic liquids, multi-ferric materials, chiral magnets and condensed matter physics in general [16] [17], [18], [19], [20], [21], [22], [23], [24] and [25]) is well recognized by now.

Recently, the generalized hedgehog ansatz introduced in [26] [27] [28] [29] [30] [31] [32] [33] [34] allowed the construction of the first analytic multi-Skyrmions at finite density as well as the first exact gravitating smooth, regular and topologically non-trivial Skyrmions configurations. Interestingly enough, very similar techniques also work very well in the case of non-Abelian monopoles [35] [36].

On the other hand, a very powerful technique to construct multi-Skyrmionic configurations in unbounded regions is given by the so-called *rational map ansatz* introduced in [15] (a detailed review is [4]). Such ansatz replaces the usual isospin vector of the standard spherical hedgehog ansatz with a more general rational map between two-spheres. Then, one can minimize the energy with respect to both the Skyrmion profile and the rational map: the resulting analytic configurations are extremely close¹ to the true numerical solutions (see, for instance, [37] [38] and references therein). Hence, the rational map ansatz is one of the most powerful analytic tools in Skyrme theory which provided, for instance, a very detailed explanation of the appearance of fullerene-like structures (as it was already argued in the original references [15] [37] [38]). Moreover, the rational map has already been tested (and with excellent results [39]) on curved backgrounds. Despite the fact that the rational map approach (unlike, for instance, the generalized hedgehog ansatz) does not produce exact solutions of the full field equations [40] (although, as already mentioned, the results are very close to the exact ones), from the field-theoretical point of view, the rational map approach to the Skyrme model can be interpreted as a way to construct exact solutions but in the mean field approximation.

One of the most intriguing (and not yet fully explored) issues related with topological charges is the analysis of their role within the AdS/CFT correspondence [41] (for a review see [42]). In this framework, the role of Noether charges of the bulk theory is quite well-understood from the boundary point of view. On the other hand, there are not so many examples of sensible bulk theories with explicit multi-solitonic solutions which are under control on the boundary. At least in the probe limit, this analysis is especially relevant in relation with the Sakai-Sugimoto model [43]. In particular, all holographic models of QCD describe baryons as topological solitons in the bulk. In the Sakai-Sugimoto model there is an identification between baryon number and instanton charge. Therefore, the construction of solitons in curved space, with a prescribed topological charge is a very relevant topic especially if the background geometry has *AdS* asymptotics. However, a bulk soliton description within holographic QCD and in particular within the Sakai-Sugimoto model is very difficult not only from the analytical but also from the numerical point of view. Nevertheless, it has been argued in [44] [45] [46] that when the density of topological charge increases, a series of phase transitions (called *popcorn transitions*) may happen. The lack of numerical computations has led to various approximate methods being employed to describe this phase, as follows. A very interesting approach has been to simplify the bulk models (decreasing the number of dimensions to 2+1: see in particular [47] [48]) in order to be able to perform a tractable numerical analysis. In this way it has been possible to discuss in detail the analogue of the popcorn transitions. These are phase transitions to multi-layered rings occurring as the topological charge (and consequently the density) increases. The motivation of the analysis carried out in this paper is to extend the above results by generalizing them to higher

¹For instance, in most cases the energies of the “rational map” multi-Skyrmions differ by less than 3 % with respect to the energies of the corresponding numerical solutions.

dimensions using the full original Skyrme model without losing the analytical and numerical control achieved in [47] [48].

In the present paper, we will first analyze the (3+1)-dimensional Skyrme model on $AdS_2 \times S_2$ using the generalized hedgehog ansatz. This analysis provides one with a framework to study the holographic meaning of topological charges in $AdS_2 \times S_2$ in a situation in which Skyrmions pile up in the radial “holographic” direction of AdS_2 (while the energy density is uniform in the S_2 directions).

Then, we will further generalize the results of the first part using the rational map formalism which is very suitable on the $AdS_2 \times S_2$ background metric. The rational map ansatz [15] will be used to construct multi-layered configurations of Skyrmions in such a way that the Skyrmions can pile up not only in the radial AdS_2 direction but also along the angular directions of S_2 . In this construction, each layer is constructed following the rational map ansatz [15] while the layers are piled up on the top of each others according to the rules determined in [26] [27] [28] [29] [30] [31] [32] [33] [34]. In the present framework, we observe the analogue of popcorn transitions in which, depending on the values of the coupling constants of the theory, for fixed total topological charge, configurations with more layers but lower densities are energetically favored over configurations made of a smaller number of layers but with higher densities.

This paper is organized as follows: in the second section the theoretical basis of the paper is introduced and reviewed, in this section we present the original model and discuss the general hedgehog ansatz applied to our particular geometry. Section 3 is devoted to a similar analysis using the rational map ansatz, we also comment on holographic popcorn transitions. In the final section, some conclusions will be drawn.

2 Generalized hedgehog

In this section, the first tool to construct analytic multi-Skyrmionic configurations [26] [27] [28] [29] [30] [31] [32] [33] [34] will be shortly described. The action S_{Sk} of the $SU(2)$ Skyrme system in four dimensional space-times is

$$S_{Sk} = \frac{K}{2} \int d^4x \sqrt{-g} \text{Tr} \left(\frac{1}{2} L^\mu L_\mu + \frac{\lambda}{16} F_{\mu\nu} F^{\mu\nu} \right) \quad K > 0, \quad \lambda > 0, \quad (1)$$

$$L_\mu := U^{-1} \nabla_\mu U = L_\mu^i t_i, \quad F_{\mu\nu} := [L_\mu, L_\nu], \quad \hbar = 1, \quad c = 1,$$

where the Planck constant and the speed of light have been set to 1, K and λ are the coupling constants, $\mathbf{1}_2$ is the 2×2 identity matrix and the t^i are the basis of the $SU(2)$ generators (where the Latin index i corresponds to the group index). The relations of the coupling constants K and λ with the couplings² F_π and e used in [10] read

$$K = \frac{1}{4} F_\pi^2, \quad K\lambda = \frac{1}{e^2}.$$

²Experimentally, $F_\pi = 186 \text{ MeV}$, from this the Skyrme constant is fitted to be $e = 5.45$.

The non-linear sigma model term of the Skyrme action is necessary to take into account pions. The second term is the only covariant term leading to a well-defined Hamiltonian formalism in time which supports the existence of Skyrmions. In the context of AdS/CFT, it has been shown that the Skyrme model appears in a very natural way [43]: we will comment more on this in the following sections.

The Skyrme field equations are

$$\nabla^\mu L_\mu + \frac{\lambda}{4} \nabla^\mu [L^\nu, F_{\mu\nu}] = 0. \quad (2)$$

The following standard parametrization of the $SU(2)$ -valued scalar $U(x^\mu)$ will be adopted

$$U^{\pm 1}(x^\mu) = Y^0(x^\mu) \mathbf{1}_2 \pm Y^i(x^\mu) t_i, \quad (Y^0)^2 + Y^i Y_i = 1. \quad (3)$$

In [27] [30] [31] [34], in order to construct multi-Skyrmionic configurations the following class of curved background has been considered:

$$ds^2 = g_{AB} dy^A dy^B + R_0^2 (d\theta^2 + (\sin \theta)^2 d\phi^2), \quad (4)$$

$$y^1 = t, \quad y^2 = r, \quad A, B = 1, 2, \quad g_{AB} = g_{AB}(t, r), \quad (5)$$

where g_{AB} is a two-dimensional metric with Lorentzian signature³. The space-times described by the above metric can be visualized as “generalized cylinders” in which the transverse sections (instead of being two-dimensional disks) are two-spheres of constant radius R_0 while the $t-r$ geometry is defined by the two-dimensional metric $g_{AB}(t, r)$. In the following analysis, R_0 will play an important role to connect the present results with the *holographic popcorn transitions* mentioned in the introduction. The reason is that R_0 can act as a control parameter to increase/decrease the charge density on the boundary of $AdS_2 \times S_2$. In particular, once a multi-Skyrmionic configuration with a prescribed topological charge on the boundary is constructed, it is possible to increase the charge density on the boundary by decreasing R_0 . In this way, we will show explicitly that popcorn-like transitions do indeed occur in our setting.

The well known result that elementary Skyrmions should be quantized as Fermions (which originally was derived on flat spaces) has been extended to space-times with compact orientable three-dimensional spatial sections in [50] (the metric in Eq. (4), which includes $AdS_2 \times S_2$ as a particular case, belongs to this class).

When g_{AB} is the two-dimensional Minkowski metric η_{AB} , it is possible to construct multiple-layer multi-Skyrmionic configurations in a finite volume without any cut-off on the coordinates. The effectiveness of this metric choice is also shown by the results in [35] [36] in which it has been shown that, unlike what happens in flat spaces, the equations for the Yang-Mills-Higgs system (in the sector with non-vanishing non-Abelian electric and magnetic charges) possess analytic solutions even in the case in which the Higgs coupling is non-zero.

The hedgehog ansatz suitable to describe a spherically symmetric Skyrmion living in the back-

³The simplest choice analyzed in that references corresponds to g_{AB} being the two-dimensional Minkowski metric η_{AB} . This case has been also considered in [49] but with different motivations.

ground of Eq. (4) is [30] [31]:

$$Y^0 = \cos \alpha , \quad Y^i = \hat{n}^i \sin \alpha , \quad \alpha = \alpha(y^A) = \alpha(r, t) , \quad (6)$$

$$\hat{n}^1 = \sin \theta \cos \phi , \quad \hat{n}^2 = \sin \theta \sin \phi , \quad \hat{n}^3 = \cos \theta . \quad (7)$$

With the above ansatz the Skyrme field equations reduce to the following scalar differential equation for the Skyrme profile α :

$$F(\alpha) D^2 \alpha + G(\alpha) (D\alpha)^2 - V(\alpha) = 0 , \quad (8)$$

$$V(\alpha) = \frac{\sin(2\alpha)}{R_0^2} \left\{ 1 + \lambda \Upsilon_0 \frac{\sin^2 \alpha}{R_0^2} \right\} , \quad \Upsilon_0 = 1 , \quad (9)$$

$$G(\alpha) = \lambda \frac{\sin(2\alpha)}{R_0^2} , \quad F(\alpha) = 1 + \frac{2\lambda}{R_0^2} \sin^2 \alpha , \quad (10)$$

$$D^2 \alpha = \frac{1}{\sqrt{-\det g_{AB}}} \partial_A \left[\sqrt{-\det g_{AB}} g^{AB} \partial_B \alpha \right] , \quad (D\alpha)^2 = g^{AB} (\partial_A \alpha) (\partial_B \alpha) ,$$

where D^2 is the D'Alembertian with respect to the two-dimensional metric g_{AB} , the coefficient Υ_0 in Eq. (9) is introduced to help the comparison with the rational map ansatz. On the other hand, the energy-density (that is, the 0-0 component of the energy-momentum tensor) reads

$$T_{00} = K \left\{ F(\alpha) \left[(\partial_t \alpha)^2 - g_{tt} \frac{(D\alpha)^2}{2} \right] - g_{tt} \frac{\sin^2 \alpha}{R_0^2} \left(1 + \lambda \frac{\sin^2 \alpha}{2R_0^2} \right) \right\} . \quad (11)$$

The winding number W for a static configuration of the form in Eqs. (6) and (7) reads:

$$W = -\frac{1}{24\pi^2} \int \epsilon^{ijk} \text{Tr} (U^{-1} \partial_i U) (U^{-1} \partial_j U) (U^{-1} \partial_k U) = -\frac{2}{\pi} \int (\alpha' \sin^2 \alpha) dx . \quad (12)$$

2.1 Generalized hedgehog on $AdS_2 \times S_2$

Here we will restrict the above formalism to the $AdS_2 \times S_2$ case. In this case, the two-dimensional metric described by g_{AB} is

$$g_{AB} dy^A dy^B = - \left(1 + \frac{r^2}{l^2} \right) dt^2 + \frac{1}{\left(1 + \frac{r^2}{l^2} \right)} dr^2 \quad (13)$$

where l is the two-dimensional AdS radius.

We will only consider static configurations:

$$\alpha = \alpha(r) , \quad (14)$$

in such a way that the full Skyrme field equations Eq. (8) reduce to:

$$\frac{-l^2 \left(1 + \lambda \frac{\Upsilon_0}{N^2} \frac{\sin^2 \alpha}{(R_0^2/N)} \right) \sin 2\alpha}{(l^2 + r^2) \left((R_0^2/N) + \lambda(1 - \cos 2\alpha) \right)} + \frac{2r}{l^2 + r^2} \alpha' + \frac{\lambda \sin 2\alpha}{R_0^2/N + \lambda(1 - \cos 2\alpha)} \alpha'^2 + \alpha'' = 0 \quad , \quad (15)$$

where in the present case in which the rational map is trivial (as we are using just the hedgehog ansatz for the isospin functions in Eq. (7)) we have

$$N = 1 \quad , \quad \frac{\Upsilon_0}{N^2} = 1 \quad . \quad (16)$$

The boundary conditions needed to find solutions with non-vanishing Baryon charge n are: $\alpha(0) = n\pi$ and $\alpha(\infty) = 0$. We find solutions to Eq.(8) with these boundary conditions numerically. Our numerical solver involves an pseudo-time relaxation procedure in which the $\alpha(r)$ profile is evolved from an initial seed which satisfies the required boundary conditions. The differential operators are discretized by a finite difference method using central differences. The accuracy of this procedure is $O(10^{-3})$. The obtained solutions are shown in figures 1 and 2 for Baryon charge up to $n = 8$.

The numerical analysis shows that there are kink-like solutions with arbitrary Baryon charge which pile up in the r direction. It is worth emphasizing that the hyperbolic geometry of AdS_2 manifests itself in figures 1 and 2. The comparison with the results in [30] (in which case the two-dimensional geometry g_{AB} was the flat Minkowski space-time) clearly shows that in the AdS_2 case the Skyrmons prefer to pile up as much as possible in a region of small r : this is a fingerprint of the “confining effect” of the AdS geometry. From the same figures (and taking into account the results in [30]), one can also see that when r is large enough ($r/l > 6$ in our units) there is no longer enough volume to fit further Skyrmons. The obvious explanation is that g_{rr} (and, correspondingly, the factor $\sqrt{g_{space}}$ which determines the volume of the $t = const$ sections of $AdS_2 \times S_2$) is very small for large r while the Skyrmion has its own natural size determined by the coupling constant of the theory. Thus, when r is too large, there simply is no space for extra Skyrmons. On the other hand, the energy-density profile along the angular direction is trivial so that a natural question arises: is it possible to probe the boundary of $AdS_2 \times S_2$ (namely, $\mathbb{R} \times S_2$) with more general multi-Skyrmionic configurations possessing non-trivial energy-density profiles along the angular directions as well? The rational map will answer this question.

3 Rational map ansatz on curved spaces

The rational map ansatz [15] achieves multi-Skyrmionic configurations replacing the isospin vector \widehat{n}^i in Eq. (7) by a more general map between two spheres. The metric in Eq. (4) can be analyzed using the rational map approach thanks to its spherical symmetry. It is worth emphasizing that the rational map ansatz is only an approximation (although a very valuable one). Consequently, the validity of all the results derived here is limited by the validity of the rational map ansatz itself. In particular, in

order for this ansatz to work, only massless Pions should be considered.

As usual for spherically symmetric backgrounds, the Skyrme field living in the metric given by Eq. (4), will be parametrized as follows

$$Y^0 = \cos \alpha , \quad Y^i = (n_R)^i \sin \alpha , \quad \alpha = \alpha(r) , \quad \delta_{ij} (n_R)^i (n_R)^j = 1 \quad (17)$$

$$(n_R)^1 = \frac{R + \bar{R}}{1 + |R|^2} , \quad (n_R)^2 = \frac{i(R - \bar{R})}{1 + |R|^2} , \quad (n_R)^3 = \frac{1 - |R|^2}{1 + |R|^2} , \quad (18)$$

$$R = R(z) , \quad z \in \mathbb{C} , \quad (19)$$

where z is a complex coordinate which, using the stereographic projection, can be identified with the coordinates on the 2-sphere:

$$z = \exp(i\phi) \tan\left(\frac{\theta}{2}\right) .$$

From the mathematical point of view, a rational map $R(z)$ is a holomorphic function from $S^2 \rightarrow S^2$. Generically, $R(z)$ can always be written as

$$R(z) = \frac{p(z)}{q(z)} ,$$

where p and q are polynomials in z with no common factor. The degree N of the rational map R is defined as

$$N = \int \frac{2idz d\bar{z}}{(1 + |z|^2)^2} \left(\frac{1 + |z|^2}{1 + |R|^2} \left| \frac{dR}{dz} \right| \right)^2 , \quad (20)$$

namely, the integrand in Eq. (20) is the pull-back of the area form on the target space sphere of the rational map R itself. It can be shown that the degree N is equal to:

$$N = \max(n_p, n_q) ,$$

where n_p and n_q are the degrees of $p(z)$ and $q(z)$ respectively. The winding number W of the configuration in Eqs. (17), (18) and (19) (which can be identified with the baryon number B even in the case of the metric in Eq. (4) as shown in [50]) reads

$$W = B = -\frac{1}{24\pi^2} \int \epsilon^{ijk} \text{Tr} (U^{-1} \partial_i U) (U^{-1} \partial_j U) (U^{-1} \partial_k U) = nN , \quad (21)$$

where

$$n = \left(-\frac{2}{\pi} \int (\alpha' \sin^2 \alpha) dx \right) , \quad (22)$$

so that the winding number is the product of the contribution coming from the profile function α (more precisely, the number of kinks along the radial direction of AdS_2 or M_2) times the degree N of the rational map R .

When

$$R = z \tag{23}$$

the rational map ansatz in Eqs. (17), (18) and (19) reduces to the hedgehog ansatz in Eq. (4) and the solution of the equation for the profile Eq. (8) provides one with an exact solution of the full Skyrme field equations. In general, the rational map allows one to describe more general configurations and, in particular, it provides one with a particularly elegant explanation of the appearance of fullerene-like structures both on flat [15] [37] [38] and curved [39] backgrounds.

The general strategy of the rational map approach⁴ is to minimize the total energy with respect to both the soliton profile and the rational map R . It is worth emphasizing that the rational map minimization procedure is a two-dimensional problem which only depends on the geometry of the two-sphere. Consequently, the numerical results obtained in [15] [37] are fully applicable in all the geometries of the form in Eq. (4). Such a strategy is known to provide excellent approximations to the full numerical solutions (see for instance, [37] [39]). One of the main advantages of this framework is that it disentangles the radial coordinate r from the angular coordinates. It is important to note that disentangling the radial coordinate is only an approximation using the rational map ansatz (although a remarkably good one for small winding numbers, at least in the cases discussed in the literature on the rational map ansatz, see for example [15] [37] [38] and [39]). Consequently, one can first minimize the energy functional with respect to the rational map (given its degree N). Then, one is left with an energy functional which only depends on the profile function so that the minimization procedure is reduced to a one-dimensional problem. The minimization of the rational map for degrees $N \leq 108$ together with the analysis of the corresponding discrete symmetries has been already performed in detail in the literature (see for instance, [37] [38] and references therein): our analysis is based on the data of [37]. In particular, we will use the results contained in table 1 page 17 of [37]. As it has been already mentioned, these results are fully applicable here as they depend only on the angular part of the metric (the S_2 part of the four dimensional manifold). Since the rational map works very well for massless Pions and not too large topological charges, in the following numerical analysis we have limited our attention to values of the Baryon charge B less than 15 (which is a range of values for B that has been well-tested in the literature on the rational map ansatz). Moreover, the rational map ansatz has been analyzed in detail on flat space-times or on curved but very regular space-times with bounded curvature. Consequently, we have chosen two background metrics ($AdS_2 \times S_2$ and $M_2 \times S_2$) which are products of constant curvature manifolds (in particular, in both cases analyzed here the curvature is globally bounded).

As an introduction (which nonetheless presents new results) we will first analyze the rational map ansatz in the simpler case of $M_2 \times S_2$ (analyzed in [30] [31] [34]) and then we will go back to the $AdS_2 \times S_2$ case.

⁴The success of this strategy is partially based on the fact that, in the case of the standard hedgehog ansatz the principle of symmetric criticality holds.

3.1 Rational map on $M_2 \times S_2$

As emphasized in [30] [31] [34], the case of $M_2 \times S_2$, which corresponds to

$$g_{tt} = -1, \quad g_{rr} = 1, \quad g_{tr} = 0, \quad -\frac{L}{2} \leq r \leq \frac{L}{2},$$

is especially suitable to describe finite-volume effects without breaking the spherical symmetry. This geometry describes a tube-shaped region whose transverse sections are two-spheres S_2 instead of disks.

The boundary conditions for the profile α in topological sector n are

$$\alpha\left(\frac{L}{2}\right) - \alpha\left(-\frac{L}{2}\right) = n\pi, \quad n \in \mathbb{Z} \quad \Leftrightarrow \quad U\left(-\frac{L}{2}\right) = (-1)^n U\left(\frac{L}{2}\right). \quad (24)$$

Hence, a configuration of the form in Eqs. (17), (18) and (19) with a profile satisfying the above boundary conditions corresponds to a Baryon number $B = nN$. One can think of these configurations as multi-layered Skyrmions made up by layers generated by the rational map ansatz such that the rule to pile up neighboring layers is determined by the procedure introduced in [30] [31] [34]. In the case of $M_2 \times S_2$, unlike what happens in the usual cases [15] [37] [38] [39], the technique introduced in [30] [31] [34] allows one to find the general solution for the equation for the Skyrmions profile, as we will shortly see.

In the present case, both the total energy of the system and the equation for the soliton profile α are simple generalizations of Eq. (8) and (11). By direct computation, one can check that the total energy is

$$E = \frac{K}{2} \int \left[F_R(\alpha) (\alpha')^2 + 2H_R(\alpha) \right] dr, \quad (25)$$

$$\Upsilon = \frac{1}{4\pi} \int \frac{2idz d\bar{z}}{(1+|z|^2)^2} \left(\frac{1+|z|^2}{1+|R|^2} \left| \frac{dR}{dz} \right| \right)^4. \quad (26)$$

where

$$F_R(\alpha) = \left(1 + \frac{2\lambda}{R_0^2} N \sin^2 \alpha \right), \quad (27)$$

$$H_R(\alpha) = \frac{\sin^2 \alpha}{R_0^2} \left(N + \frac{\lambda}{2R_0^2} \Upsilon \sin^2 \alpha \right). \quad (28)$$

while, the equation for the Skyrmion profile $\alpha(r)$ reads

$$F_R(\alpha) \alpha'' + \frac{1}{2} \frac{d}{d\alpha} (F_R(\alpha)) (\alpha')^2 - V_R(\alpha) = 0, \quad (29)$$

$$V_R(\alpha) = \frac{N \sin(2\alpha)}{R_0^2} \left\{ 1 + \lambda \frac{\Upsilon \sin^2 \alpha}{N R_0^2} \right\}. \quad (30)$$

It is interesting to compare the rational map ansatz and, in particular, Eqs. (29), (27), (28) and (30) with the corresponding equations for the standard hedgehog ansatz at finite volume in [30]. It is clear that the rational map ansatz corresponds to the following rescalings on R_0 and Υ_0 in Eqs. (8), (9) and (10):

$$R_0^2 \rightarrow \bar{R}^2 = \frac{R_0^2}{N}, \quad \Upsilon_0 \rightarrow \eta = \frac{\Upsilon}{N^2}, \quad (31)$$

namely, the rational map decreases the effective area of the sections of the tube by a factor $1/N$ (so that \bar{R}^2 in Eq. (31) represents the area “available” for elementary Skyrmions in each layer) while the effective coupling η induced by the rational map is the integral Υ defined in Eq. (26) divided by N^2 .

Interestingly Υ grows roughly⁵ as N^2 (see, for instance, the numerical results in [37] [38]) and consequently η is a quite natural effective coupling constant. The present notations map into the ones of [37] as follows. The integral Υ (defined in Eq. (26)) in the above equations corresponds to the quantity “ I ” (which appears in the third column of table 1 page 17 of [37]) while the degree of the rational map N (defined in Eq. (20)) corresponds to the quantity “ B ” (which appears in the first column of table 1 page 17 of [37]). Therefore, the relevant quantity η defined in Eq. (31) appears in the fourth column of table 1 page 17 of [37]. These values of [37] will be used in the numerical analysis of the following sections.

The minimization procedure for the rational map R corresponds to minimizing the integral Υ in Eq. (26) subject to the constraint that the degree of the rational map in Eq. (20) is N (see for instance, [37] [39] and references therein). Hence, one can see that the effect of the rational map ansatz can be interpreted as the rescaling in Eq. (31) of the coupling constants appearing in the field equation (8) for the profile in the case of the standard hedgehog ansatz. Also in the case of the rational map, the equation (29) for the profile can be solved as follows

$$(\alpha')^2 = \frac{I_c + 2H_R(\alpha)}{F_R(\alpha)}, \quad (32)$$

where I_c is an integration constant. The dependence of the integration constant I_c on the number of layers n is determined by the following condition

$$\frac{L}{n} \stackrel{def}{=} l_{eff} = \pm \int_0^\pi \sqrt{\frac{F_R(\alpha)}{I_c + 2H_R(\alpha)}} d\alpha, \quad (33)$$

where for definiteness we will consider only the $+$ sign in the above equation and l_{eff} (which is the total length of the tube divided by the number of layers) is the effective length available for each layer along the r -direction. It can be easily shown that this equation for I_c always has a smooth regular solution with $I_c \geq 0$.

⁵According to all the available numerical data (see [37] [38] and references therein), in the large N limit the effective coupling η defined in Eq. (31) has a smooth behavior (at least until $N = 108$) staying almost constant, or slowly decreasing, when N is large. The fact that Υ is of order N^2 can also be understood by comparing the definition of N in Eq. (20) with the definition of Υ in Eq. (26).

A non-trivial BPS bound can also be derived:

$$E_{tot} \geq |Q_R| , \quad (34)$$

$$Q_R = 4\sqrt{2}\pi R_0^2 K \int_0^\pi [F_R(\alpha)H_R(\alpha)]^{1/2} d\alpha . \quad (35)$$

One of the most important consequences of the fact that the equation (29) for the profile can be solved by quadrature as in Eq. (32) is that it allows one to derive a closed explicit form for the total energy of the system as a function of the couplings of the theory K and λ , of the geometric parameters R_0 and L characterizing the tube-shaped domain, and of n and N which are the number of layers and the number of particles for each layer respectively. In principle, this allows a detailed and explicit thermodynamical analysis of the system in which the explicit knowledge of the dependence of the Skyrme profile α on r is not needed at all. This can be seen as follows. One needs the explicit dependence of the total energy on the parameters of the system which are K , λ , R_0 , L as well as on the Baryon number and on the rational map degree. At first glance, in order to achieve this goal one needs to know $\alpha(r)$ and then to plug the expression into Eq. (25) to reach the desired expression for the total energy. However, a simple trick provides us with the sought expression without the knowledge of $\alpha(r)$. Indeed, from Eq. (32) we get

$$dr = \left[\frac{F_R(\alpha)}{I_c + 2H_R(\alpha)} \right]^{1/2} d\alpha$$

and using the above expression to eliminate dr from Eq. (25) one obtains

$$E = \frac{K}{2} \int_0^{n\pi} [I_c + 4H_R(\alpha)] \left[\frac{F_R(\alpha)}{I_c + 2H_R(\alpha)} \right]^{1/2} d\alpha , \quad (36)$$

where n is the number of kinks along the radial direction r . Thus, taking into account that I_c is defined in Eq. (33), the above equation represents an explicit expression for the total energy of the system as a function of K , λ , R_0 , L as well as of n and N . For instance, one can derive the above expression with respect to L and R_0 to obtain explicit expressions for the longitudinal and radial pressures (namely, $\frac{\partial E}{\partial L}$ and $\frac{\partial E}{\partial R_0}$). It is also worth mentioning that for suitable values of I_c Eq. (36) can be reduced to an elliptic integral [51]. We will not analyze this case in detail and focus on the more interesting case of $AdS_2 \times S_2$ (in which, however, numerical analysis is needed).

3.2 Rational map on $AdS_2 \times S_2$

Here we will apply the same procedure to $AdS_2 \times S_2$. Namely, the Skyrme field living in the metric in Eq. (13), will be parametrized using Eqs. (17), (18) and (19). Then, the second step of the method is to minimize the total energy with respect to both the soliton profile and the rational map R . By

doing this, one obtains for static configurations the following equation for the profile

$$F_R(\alpha) \partial_r \left(\left(1 + \frac{r^2}{l^2} \right) \partial_r \alpha \right) + \frac{1}{2} \frac{d}{d\alpha} (F_R(\alpha)) \left(1 + \frac{r^2}{l^2} \right) (\alpha')^2 - V_R(\alpha) = 0 \quad , \quad (37)$$

with the same rescaling as in Eqs. (27), (30) and (31). Indeed, it is easy to check that this equation can be written in the form

$$\frac{-l^2 \left(1 + \lambda \eta \frac{\sin \alpha^2}{(R_0^2/N)} \right) \sin 2\alpha}{(l^2 + r^2) \left((R_0^2/N) + \lambda(1 - \cos 2\alpha) \right)} + \frac{2r}{l^2 + r^2} \alpha' + \frac{\lambda \sin 2\alpha}{R_0^2/N + \lambda(1 - \cos 2\alpha)} \alpha'^2 + \alpha'' = 0 \quad , \quad (38)$$

where η is given by Eq. (31). The numerical values of the coupling η for many values of the degree N of the rational map as well as the corresponding discrete symmetries can, once again, be found in table 1 page 17 of [37]. This equation should be compared to equation (15) which corresponds to the trivial rational map. We see that the equations are extremely similar, this is why the constant $\Upsilon = 1$ was introduced previously. The numerical constants in the latter equation are different from unity, corresponding to different degrees of the rational map. However, the general form of the solutions will be identical, hence we refer the reader to figures 1 and 2 for the general form of the soliton profiles.

Thus, as before, we conclude that the rational map decreases the effective area available for the Skyrmons of the ($r = \text{const}$, $t = \text{const}$) sections of $AdS_2 \times S_2$ by a factor $1/N$. On the other hand, the rational map induces the effective coupling η through integral Υ defined in Eq. (26) divided by N^2 (see, Eq. (31)).

3.3 Holographic-popcorn interpretation

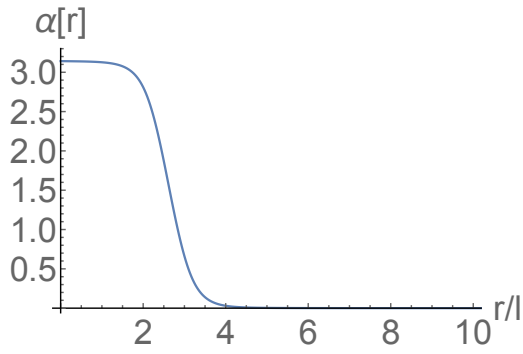
The possibility to use the generalized hedgehog ansatz [26] [27] [28] [30] [31] [33] [34] together with the rational map formalism [15] [37] [38] [39] on $AdS_2 \times S_2$ allows one to ask the following natural and interesting question:

Given a set of values for the parameters of the theory (namely, K , λ and R_0) and a fixed total Baryon number

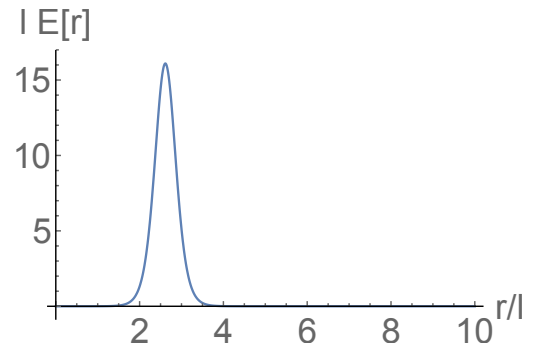
$$B = -\frac{1}{24\pi^2} \int \epsilon^{ijk} Tr (U^{-1} \partial_i U) (U^{-1} \partial_j U) (U^{-1} \partial_k U) = nN$$

(which, as explained in Eq. (21), is the product of the “number of kinks” along the radial AdS_2 direction times the degree of the rational map N), is it energetically more convenient to have higher N and lower n or instead lower N and higher n ?

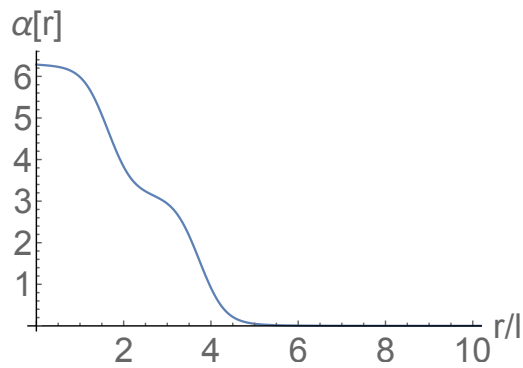
This question has many features in common with the holographic popcorn transitions [44] [45] [46]. In those references, it is argued that with increasing density a series of transitions takes place where the solitons crystal develops additional layers in the holographic direction. A very similar phenomenon was investigated in 2+1 dimensions in [47] [48]. In the recent publication [52], the author (in a low-dimensional toy version of the Sakai-Sugimoto model) discovered the “existence of further popcorn transitions to three layers and beyond”. It seems that these findings are quite consistent with the present results obtained in the (3+1)-dimensional Skyrme model within the rational map approx-



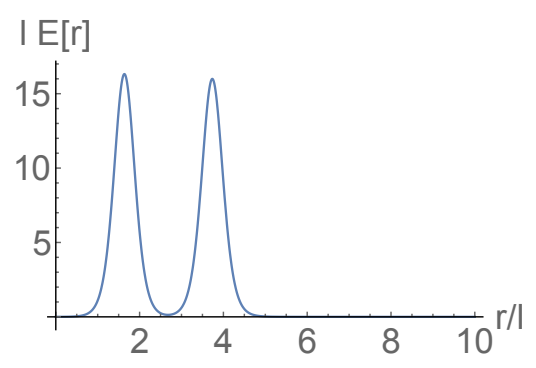
(a)



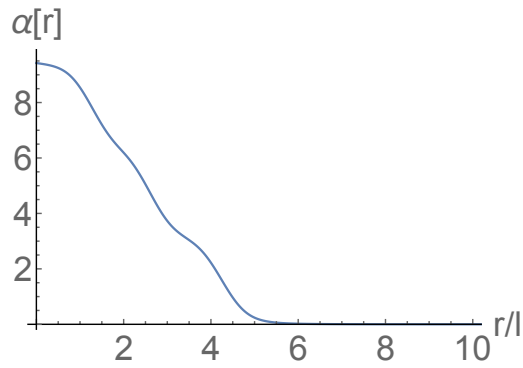
(b)



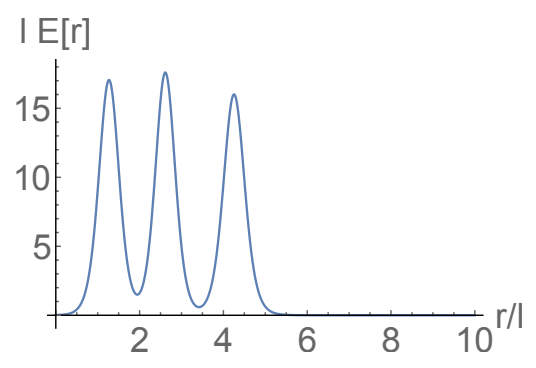
(c)



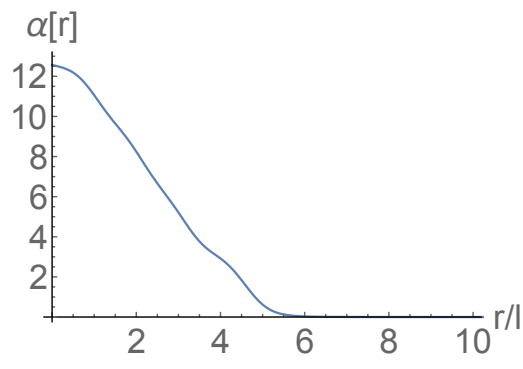
(d)



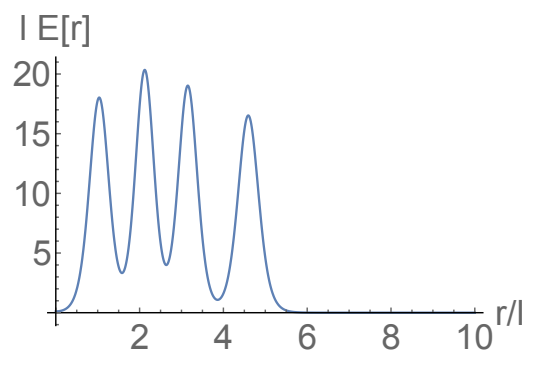
(e)



(f)



(g)



(h)

Figure 1: Solution profiles, alongside their respective energy profiles, at (in units of $l = 1$) $\lambda = 0.1$, $R_0 = 0.4$, $N = 1$, $\Upsilon = 1$ and $K = 1$, for $n = 1$ up to $n = 4$.

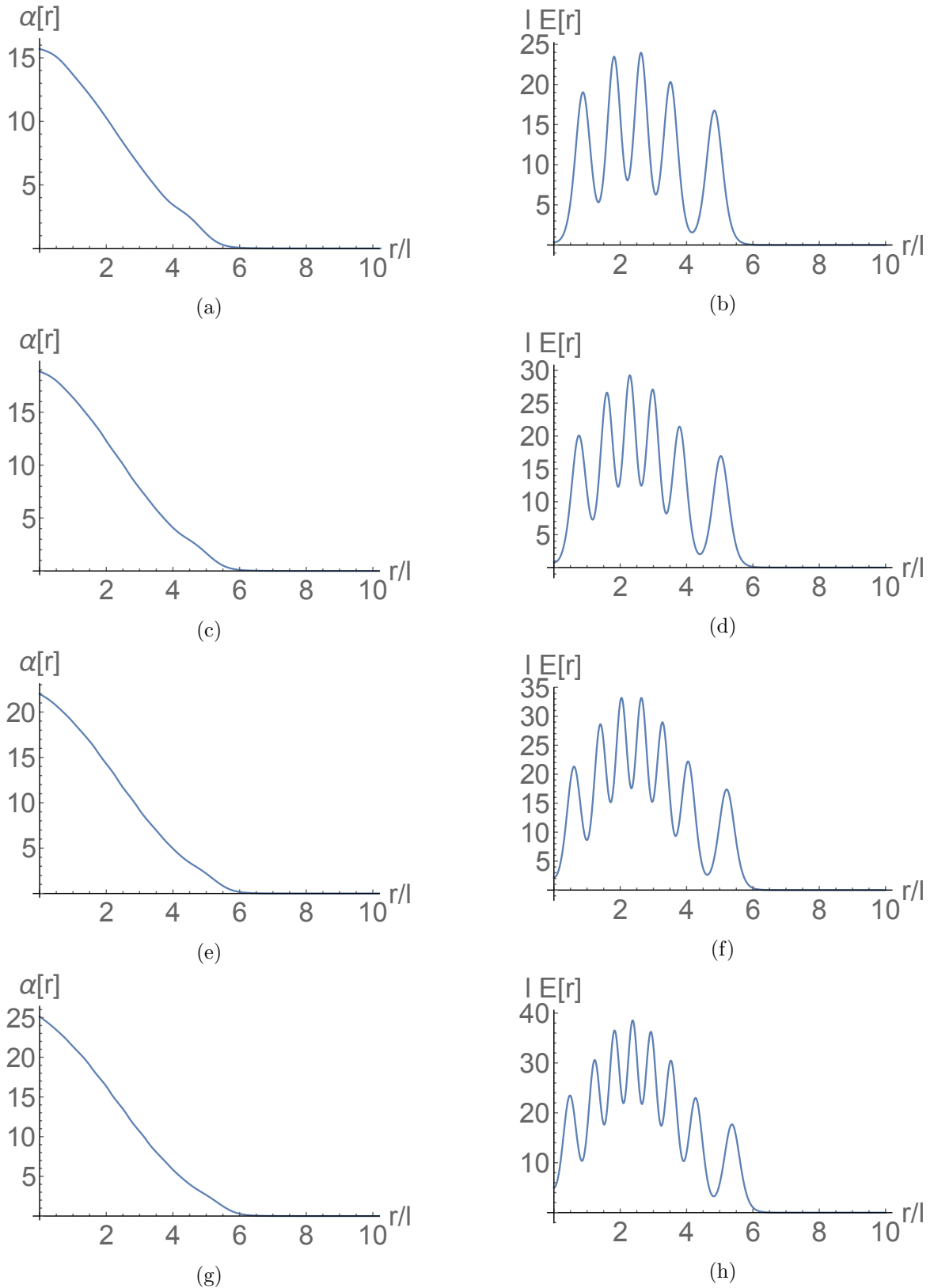


Figure 2: Solution profiles, alongside their respective energy profiles, at (in units of $l = 1$) $\lambda = 0.1$, $R_0 = 0.4$, $N = 1$, $\Upsilon = 1$ and $K = 1$, for $n = 5$ up to $n = 8$.

imation in which transitions to multi-layers configurations are explicitly observed. This reductions in dimensions is a clear avenue to maintain numerics under suitable control.

Here we observe directly in 3+1 dimensions this kind of phenomenon in the case in which the geometry is $AdS_2 \times S_2$. A useful technical feature of the present framework is that R_0 in Eq. (4) acts as a control parameter allowing to increase/decrease the charge density on the boundary (see the comments below Eq. (4)). The equation for the profile (see Eqs. (15) and (38)) produces kinks in the radial “holographic” direction. One should visualize (since the geometry is a product $AdS_2 \times S_2$) the situation as follows: at the position r_i of each kink (where $i = 1, \dots, n$) in the radial direction there is a layer (extending in the θ - φ directions of S_2) made of N “rational lumps”. Such rational lumps (which are piled up along the holographic radial direction) are characterized by discrete symmetries: here we will only consider the discrete symmetries analyzed in [37]. In each layer, the density is $\frac{N}{R_0^2}$ so that, for fixed R_0 , increasing the degree N of the rational map means increasing the density in each layer and, in particular, on the boundary of the manifold which is

$$\partial(AdS_2 \times S_2) = \mathbb{R}_t \times S_2 .$$

Correspondingly, one expects that if the density in each layer is too high, it is energetically favorable to decrease the well-known Skyrminion repulsion and to have more kinks (namely, more layers) but with a lower N .

The numerical results, presented in a separate page, confirm quite clearly the “popcorn pattern” mentioned above. We present our numerical results in the tables shown in figures 3 and 4 for some characteristic topological number combinations. We introduce the notation T_{abcd} indicating we are taking the energy difference between the sectors with topological charge ab , where $a = n$ and $b = N$, and those with the same charge $cd = ab$, where once again $c = n$ and $d = N$. The values of the effective coupling η in Eq. (38) (together with the corresponding discrete symmetries of the rational lumps) for each value of N can be read in the fourth column of table 1 page 17 of [37]. The most striking display of this behavior can be seen in figure 4.

In the case presented in figure 3 (c) the charge density on the boundary is 64 times smaller then in the case described in figure 3 a). Correspondingly, as shown in 4, one can distinctly see that (no matter the discrete symmetry of the rational lumps⁶) the most energetically convenient configuration is the one with the least number of peaks in the radial AdS_2 direction and that the energy increases by increasing the number of radial peaks (namely, n).

On the other hand, for larger charge density, one can distinctly see that (almost always) the most energetically convenient configuration is the one with the maximum number of allowed peaks (for given total Baryon charge) and that the energy increases by decreasing the number of radial peaks.

Thus, the present results show convincingly in a (3+1)-dimensional setting that, as the charge density on the boundary increases, it becomes more and more convenient to have multi-layered configurations in which the layers have low charge.

⁶Such discrete symmetries can be read in [37].

nN		$l\Delta E$
2	$T_{12;21}$	2.423
4	$T_{14;41}$	8.893
4	$T_{14;22}$	4.048
4	$T_{41;22}$	-4.846
6	$T_{16;61}$	20.345
6	$T_{16;32}$	13.084
6	$T_{16;23}$	8.541
6	$T_{61;23}$	-11.804
6	$T_{61;32}$	-7.261
6	$T_{23;32}$	4.543
8	$T_{18;81}$	32.417
8	$T_{18;42}$	22.811
8	$T_{18;24}$	14.715
8	$T_{81;24}$	-17.701
8	$T_{81;42}$	-9.606
8	$T_{24;42}$	8.095
12	$T_{1,12;12,1}$	62.736
12	$T_{12,1;43}$	-22.359
12	$T_{12,1;34}$	-25.416
12	$T_{12,1;62}$	-13.273
12	$T_{12,1;26}$	-39.455
12	$T_{1,12;43}$	40.377
12	$T_{1,12;34}$	37.320
12	$T_{1,12;62}$	49.463
12	$T_{1,12;26}$	23.282
12	$T_{34;43}$	3.057
12	$T_{34;26}$	-14.039
12	$T_{34;62}$	12.143
12	$T_{43;26}$	-17.096
12	$T_{43;62}$	9.086
12	$T_{26;62}$	26.181

(a) $R_0 = 0.1$

nN		$l\Delta E$
2	$T_{12;21}$	-0.063
4	$T_{14;41}$	-0.355
4	$T_{14;22}$	0.162
4	$T_{41;22}$	0.518
6	$T_{16;61}$	-0.942
6	$T_{16;32}$	1.327
6	$T_{16;23}$	1.062
6	$T_{61;23}$	2.004
6	$T_{61;32}$	2.268
6	$T_{23;32}$	0.265
8	$T_{18;81}$	-2.744
8	$T_{18;42}$	2.494
8	$T_{18;24}$	2.360
8	$T_{81;24}$	5.104
8	$T_{81;42}$	5.238
8	$T_{24;42}$	0.134
12	$T_{1,12;12,1}$	-10.128
12	$T_{12,1;43}$	16.357
12	$T_{12,1;34}$	16.548
12	$T_{12,1;62}$	15.571
12	$T_{12,1;26}$	14.336
12	$T_{1,12;43}$	6.229
12	$T_{1,12;34}$	6.420
12	$T_{1,12;62}$	5.443
12	$T_{1,12;26}$	4.208
12	$T_{34;43}$	-0.192
12	$T_{34;26}$	-2.213
12	$T_{34;62}$	-0.977
12	$T_{43;26}$	-2.021
12	$T_{43;62}$	-0.786
12	$T_{26;62}$	1.235

(b) $R_0 = 0.4$

nN		$l\Delta E$
2	$T_{12;21}$	-1.281
4	$T_{14;41}$	-6.869
4	$T_{14;22}$	-1.375
4	$T_{41;22}$	5.494
6	$T_{16;61}$	-16.387
6	$T_{16;32}$	-3.108
6	$T_{16;23}$	-1.180
6	$T_{61;23}$	15.206
6	$T_{61;32}$	13.279
6	$T_{23;32}$	-1.928
8	$T_{18;81}$	-31.614
8	$T_{18;42}$	-5.791
8	$T_{18;24}$	-0.792
8	$T_{81;24}$	30.822
8	$T_{81;42}$	25.823
8	$T_{24;42}$	-4.999
12	$T_{1,12;12,1}$	-79.427
12	$T_{12,1;43}$	74.930
12	$T_{12,1;34}$	78.058
12	$T_{12,1;62}$	64.905
12	$T_{12,1;26}$	79.178
12	$T_{1,12;43}$	-4.497
12	$T_{1,12;34}$	-1.369
12	$T_{1,12;62}$	-14.522
12	$T_{1,12;26}$	-0.249
12	$T_{34;43}$	-3.127
12	$T_{34;26}$	1.120
12	$T_{34;62}$	-13.153
12	$T_{43;26}$	4.248
12	$T_{43;62}$	-10.025
12	$T_{26;62}$	-14.273

(c) $R_0 = 0.8$

Figure 3: Energy differences between topological sectors T_{abcd} indicating we are taking the energy difference between the sectors with topological charge ab , where $a = n$ and $b = N$, and those with charge cd , where once again $c = n$ and $d = N$. We present in the tables the energy differences for overall topological charges 2, 4, 6, 8, 12. All values are at (in units of $l = 1$) $\lambda = 0.1$, and $K = 1$.

nN	R_0	E^*
2	0.1	T_{21}
2	0.4	T_{12}
2	0.8	T_{12}
4	0.1	T_{41}
4	0.4	T_{22}
4	0.8	T_{14}
6	0.1	T_{61}
6	0.4	T_{32}
6	0.8	T_{16}
8	0.1	T_{81}
8	0.4	T_{42}
8	0.8	T_{18}
12	0.1	$T_{12,1}$
12	0.4	T_{34}
12	0.8	$T_{1,12}$

Figure 4: Preferred energy configurations E^* per topological sector as R_0 is varied.

4 Conclusions

In the present paper, multi-Skyrmions of the four-dimensional Skyrme model are constructed on $AdS_2 \times S_2$. In order to achieve this goal, two different techniques have been combined. The first one is the generalized hedgehog ansatz while the second one is the well known rational map ansatz. The advantage of the present geometrical setting is that, even without going into a lower-dimensional theory, numerical analysis of multi-solitons can be performed (at finite density too) easily. We have shown that it is possible to solve numerically the equation for the Skyrme profile for any degree of the rational map. The present results give strong evidence for the correctness of the popcorn transition pattern. However, this should ideally be checked by a full 3-D numerical calculation. Moreover, we have also discussed that case of $M_2 \times S_2$. Our results compare nicely with the ones in the existing literature on the subject. In particular, in [48] and [47] the authors analyzed holographic popcorn transitions within the baby Skyrme model in a pure 3d AdS background. The low dimensionality of the model makes full numerical field computations viable. The main price to pay (besides the low dimensionality) is the fact that, instead of using the original 4d Skyrme model (related to the low energy limit of QCD), they used the 3d baby Skyrme model which is a toy model. The advantage of the approach presented here is that we can analyze the original 4d Skyrme model on a four-dimensional background with a clear holographic direction (namely, $AdS_2 \times S_2$). Our results give strong evidence for the correctness of the holographic popcorn transition. The price we have pay in turn for the gain in dimensionality and for the possibility to use the 4d Skyrme model is the rational map ansatz which, in general, only produces approximated results.

Acknowledgements

This work has been funded by the Fondecyt grants 1160137, 3140122. The Centro de Estudios Científicos (CECs) is funded by the Chilean Government through the Centers of Excellence Base Financing Program of Conicyt.

References

- [1] J. Myrheim, "Anyons" in "Topological aspect of low-dimensional systems", Les Houches, Session LXIX, A. Comtet, T. Jolicœur, S. Ouvry, F. David editors.
- [2] T. Skyrme, *Proc. R. Soc. London A* **260**, 127 (1961); *Proc. R. Soc. London A* **262**, 237 (1961); *Nucl. Phys.* **31**, 556 (1962).
- [3] H. Weigel, *Chiral Soliton Models for Baryons*, (Springer Lecture Notes 743)
- [4] N. Manton and P. Sutcliffe, *Topological Solitons*, (Cambridge University Press, Cambridge, 2007).
- [5] M. Shifman, A. Yung, "Supersymmetric Solitons" Cambridge University Press, (2009).
- [6] David I. Olive and Peter C. West (Editors), *Duality and Supersymmetric Theories*, (Cambridge University Press, Cambridge, 1999).
- [7] A.P. Balachandran, H. Gomm, R.D. Sorkin, *Nucl. Phys.* **B 281** (1987), 573-612.
- [8] A.P. Balachandran, A. Barducci, F. Lizzi, V.G.J. Rodgers, A. Stern, *Phys. Rev. Lett.* **52** (1984), 887.
- [9] A.P. Balachandran, F. Lizzi, V.G.J. Rodgers, A. Stern, *Nucl. Phys.* **B 256**, (1985), 525-556.
- [10] G. S. Adkins, C. R. Nappi, E. Witten, *Nucl. Phys.* **B 228** (1983), 552-566.
- [11] E. Guadagnini, *Nucl. Phys.* **B 236** (1984), 35-47.
- [12] A.P. Balachandran, G. Marmo, B. S. Skagerstam, A. Stern, "Classical Topology and Quantum States" World Scientific, 1991.
- [13] N. S. Manton, *Phys. Lett.* **110B**, 54 (1982).
- [14] Y. M. Cho, *Phys. Rev. Lett.* **87** (2001), 252001.
- [15] C. J. Houghton, N. S. Manton, P. M. Sutcliffe, *Nucl. Phys.* **B 510**, 507 (1998).
- [16] H. Pais, J. R. Stone, *Phys. Rev. Lett.* **109** (2012), 151101.
- [17] Al Khawaja, Usama; Stoof, Henk., *Nature* **411** (2001): 918-20.
- [18] J.-I. Fukuda, S. Zumer, *Nature Communications* **2** (2011), 246.

- [19] Christian Pfeiderer, Achim Rosch, *Nature* **465**, 880–881 (2010).
- [20] S. Mühlbauer, B. Binz, F. Jonietz, C. Pfeiderer, A. Rosch, A. Neubauer, R. Georgii, P. Böni, *Science* **323** (2009), pp. 915-919
- [21] F. Jonietz, S. Mühlbauer, C. Pfeiderer, A. Neubauer, W. Münzer, A. Bauer, T. Adams, R. Georgii, P. Böni, R. A. Duine, K. Everschor, M. Garst, A. Rosch, *Science* **330** (2010), 1648.
- [22] S. Seki, X. Z. Yu, S. Ishiwata, Y. Tokura, *Science* **336** (2012), pp. 198-201.
- [23] U. K. Roessler, A. N. Bogdanov, C. Pfeiderer, *Nature* **442**, 797 (2006).
- [24] A. N. Bogdanov D. A. Yablonsky, *Sov. Phys. JETP* **68**, 101 (1989).
- [25] A. Bogdanov, A. Hubert, *J. Magn. Magn. Mater.* **138**, 255 (1994); **195**, 182 (1999).
- [26] F. Canfora, P. Salgado-Rebolledo, *Phys. Rev. D* **87**, 045023 (2013).
- [27] F. Canfora, H. Maeda, *Phys. Rev. D* **87**, (2013) 084049.
- [28] F. Canfora, *Phys. Rev. D* **88**, (2013), 065028.
- [29] S. Chen, Y. Li, Y. Yang, *Phys. Rev. D* **89** (2014), 025007.
- [30] F. Canfora, F. Correa, J. Zanelli, *Phys. Rev. D* **90**, 085002 (2014).
- [31] F. Canfora, M. Di Mauro, M. A. Kurkov, A. Naddeo, *Eur. Phys. J. C* **75** (2015) 9, 443.
- [32] S. Chen, Y. Yang, *Nucl. Phys. B* **904** (2016) 470.
- [33] E. Ayon-Beato, F. Canfora, J. Zanelli, *Phys. Lett. B* **752**, (2016) 201-205.
- [34] F. Canfora, G. Tallarita, *Phys. Rev. D* **94** (2016), 025037.
- [35] F. Canfora, G. Tallarita, *Phys. Rev. D* **91** (2015), 085033
- [36] F. Canfora, G. Tallarita, *JHEP* **1409** (2014) 136.
- [37] R. A. Battye, P. M. Sutcliffe, *Rev. Math. Phys.* **14**, 29 (2002).
- [38] P.H.C. Lau, N.S. Manton, "Quantization of T_d - and O_h -symmetric Skyrmions" *Phys.Rev.* D89 (2014) no.12, 125012.
- [39] S. Krusch, " S^3 Skyrmions and the Rational Map Ansatz" *Nonlinearity* 13 (2000) 2163.
- [40] C. J. Houghton and S. Krusch, "Folding in the Skyrme model," *J. Math. Phys.* **42**, 4079 (2001)
- [41] J. Maldacena, *Advances in Theoretical and Mathematical Physics* **2**: 231–252, (1998).
- [42] O. Aharony, S. Gubser, J. Maldacena, H. Ooguri, Y. Oz, "Large N Field Theories, String Theory and Gravity". *Phys. Rept.* 323 (3–4): 183–386 (2000).

- [43] T. Sakai and S. Sugimoto, *Prog. Theor. Phys.* **113**, 843 (2005).
- [44] M. Rho, S. -J. Sin and I. Zahed, *Phys. Lett. B* 689 (2010) 23.
- [45] V. Kaplunovsky, D. Melnikov and J. Sonnenschein, *JHEP* 1211 (2012) 047.
- [46] V. Kaplunovsky and J. Sonnenschein, " *Dimension Changing Phase Transitions in Instanton Crystals*" *JHEP* 1404 (2014) 022.
- [47] S. Bolognesi, P. Sutcliffe, *A low-dimensional analogue of holographic baryons*, *J.Phys. A*47 (2014) 135401.
- [48] M. Elliot-Ripley, T. Winyard, *Baby Skyrmions in AdS*, *JHEP* 1509 (2015) 009.
- [49] L. Bratek, *Phys. Rev. D* **78**, 025019 (2008).
- [50] D. Auckly, J. M. Speight, *Comm. Math. Phys* **263** (2006) 173.
- [51] C. Adam, C. Naya, J. Sanchez-Guillen, J. M. Speight and A. Wereszczynski, *Phys. Rev. D* **90**, 045003 (2014)
- [52] M. Elliot-Ripley, *J. Phys. A* **50**, no. 14, 145401 (2017).